

# Energy & Environmental Science

Accepted Manuscript



This is an *Accepted Manuscript*, which has been through the Royal Society of Chemistry peer review process and has been accepted for publication.

*Accepted Manuscripts* are published online shortly after acceptance, before technical editing, formatting and proof reading. Using this free service, authors can make their results available to the community, in citable form, before we publish the edited article. We will replace this *Accepted Manuscript* with the edited and formatted *Advance Article* as soon as it is available.

You can find more information about *Accepted Manuscripts* in the [Information for Authors](#).

Please note that technical editing may introduce minor changes to the text and/or graphics, which may alter content. The journal's standard [Terms & Conditions](#) and the [Ethical guidelines](#) still apply. In no event shall the Royal Society of Chemistry be held responsible for any errors or omissions in this *Accepted Manuscript* or any consequences arising from the use of any information it contains.

Cite this: DOI: 10.1039/c0xx00000x

ARTICLE TYPE

www.rsc.org/xxxxxx

## Membrane-less electrolyzer for hydrogen production across the pH scale

Seyyed Mohammad Hosseini Hashemi,<sup>a</sup> Miguel A. Modestino<sup>a</sup> and Demetri Psaltis<sup>\*a</sup>

Received (in XXX, XXX) Xth XXXXXXXXXX 20XX, Accepted Xth XXXXXXXXXX 20XX

DOI: 10.1039/b000000x

5 The development of deployable water-splitting devices is hindered by the lack of stable ion conducting membranes that can operate across the pH scale, impose low ionic resistances and avoid product mixing. The membrane-less approach developed in this work breaks this paradigm and demonstrates for the first time an electrolyzer capable of operating with lower ionic resistance than benchmark membrane-based electrolyzers using virtually any electrolyte. Our method separates product gases by controlling the  
10 delicate balance between fluid mechanic forces in the device. The devices presented here are able to split water at current densities over 300 mA/cm<sup>2</sup>, with more than 42% power conversion efficiency, and crossover of hydrogen gas into the oxidation side as low as 0.4%, leading to a non-flammable and continuous hydrogen fuel stream. Furthermore, being able to use buffered electrolytes allows for the incorporation of earth-abundant catalysts that can only operate at moderate to high pH.

### 15 Introduction

Hydrogen gas is a clean alternative fuel which has the potential to redefine our fossil-fuel based infrastructure if its production cost reached levels competitive with conventional energy resources. As the only emission from hydrogen-based energy production is  
20 water, the adoption of this fuel can alleviate many environmental concerns. Furthermore, the use of hydrogen as a vehicle for energy storage can enable the large-scale deployment of renewable energy sources such as solar and wind which suffer from their intermittent availability. Currently, most of the  
25 hydrogen produced in the world comes from steam reforming of natural gas<sup>1</sup>, a process that intrinsically releases at least 1 molecule of CO<sub>2</sub> for every 3 molecules of H<sub>2</sub> produced. A truly clean alternative is to use renewable energy sources, to drive water electrolysis systems and store the excess energy as H<sub>2</sub> fuel.  
30 State-of-the-art electrolysis systems are based on membrane electrode assemblies (MEAs) that take advantage of low ionic resistance through Nafion<sup>®</sup> membranes that separate the hydrogen and oxygen evolution sites<sup>2-4</sup>. Although membranes allow for production of nearly-pure gas streams and the operation  
35 of electrolyzers at high current densities, the strongly acidic nature of Nafion requires the incorporation of acid-stable catalysts that are based on noble metals, i.e. Pt and Ir<sup>5</sup>. The lack of stable and high-performing membranes that operate under basic and near-neutral conditions has precluded the incorporation

40 of practical earth-abundant water splitting catalysts or photocatalytic materials into deployable devices<sup>6-14</sup>, as they have limited stability under acidic electrolytes. Research on anion-conducting membranes have led to promising alternatives for operation at high pH<sup>15-21</sup>, but their implementation in  
45 electrochemical devices lags behind Nafion. Even more complex issues arise for devices operated under near-neutral conditions<sup>22, 23</sup>, where stable operation is possible only by the implementation of controlled convective flows together with ion-conduction by a supporting electrolyte<sup>24</sup>. Membrane-less electrolysis can allow for  
50 the operation of devices at any pH, reduce the complexity by the elimination of separation membranes and decrease the ionic resistance thanks to the higher ion-mobility in liquid electrolytes<sup>25</sup>. Membrane-less designs have been previously used in other electrochemical devices such as fuel cells<sup>26-33</sup> and  
55 batteries<sup>34, 35</sup>. However, there is a fundamental difference in water electrolysis where gaseous products (hydrogen and oxygen) evolve out of the liquid electrolyte. The consequent bubble formation at the electrodes is problematic as it enhances product mixing and slows down the reaction. This is a significant  
60 challenge that has precluded demonstrations of efficient membrane-less electrolyzers in the past. To mitigate gas crossover in a membrane-less scheme, fluid dynamic approaches can be implemented in order to control the position and trajectory of gas bubbles as they evolve from electrodes (Fig. 1).

Cite this: DOI: 10.1039/c0xx00000x

www.rsc.org/xxxxxx

ARTICLE TYPE

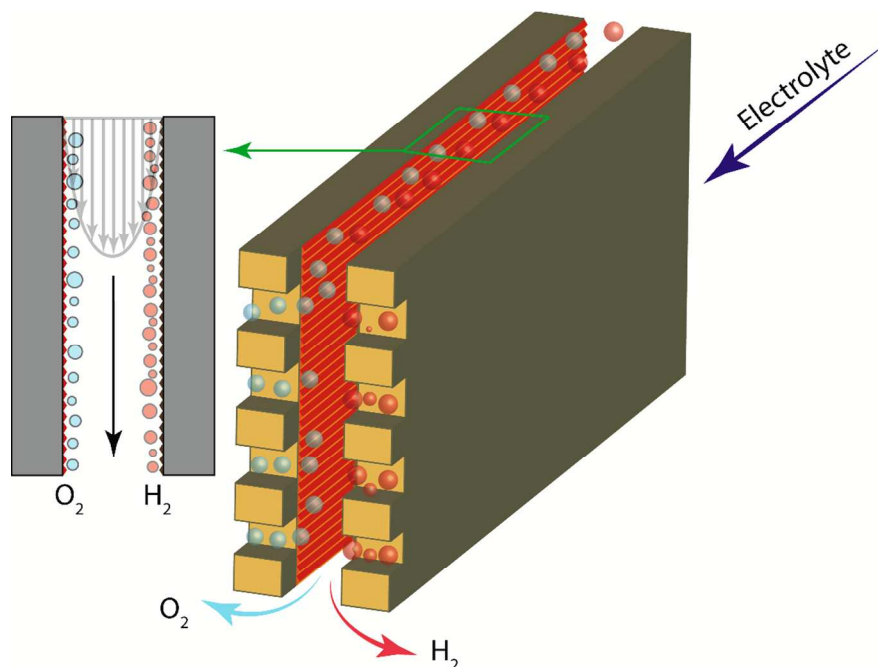


**Fig. 1** Schematic diagram of the membrane-less electrolysis: two parallel plates are coated with hydrogen and oxygen evolution catalysts, respectively and are separated by less than few hundreds of micrometers. The electrolyte flows between the catalyst plates and the evolved gases move close to the corresponding catalyst surface due to the Segré-Silberberg effect. Each of the product gas streams is collected in dedicated outlets. Stacks of these planes in horizontal can be used for higher throughput.

Previous studies on internal laminar flow of solid particles' suspensions<sup>36-40</sup> have demonstrated that the particles line up at an off-center position which is velocity dependent, a phenomenon known as the Segré-Silberberg effect<sup>41</sup>. This effect is observed because the fluidic velocity gradient across the particles' body exerts a net inertial lift force on them towards the wall, which is counteracted by a force generated by the high pressure field that forms between the particles and the channel wall. The balance of these two forces determines the equilibrium position of the particles in the channel, which controls its trajectory. This phenomenon attracted enormous attention in the microfluidics community where precise control of the particles in microchannels is desirable. This effect combined with geometrically induced forces can be directly implemented in applications that require particle separation, focusing, sorting, or filtering<sup>42-44</sup>. Non-rigid entities such as bubbles and droplets, experience an additional lift force due to deformability which directs them away from the wall<sup>45</sup>. This additional force causes the bubble's equilibrium position to be farther from the wall than for rigid spheres, and can only be overcome by increasing the flow rates in order to keep the bubbles away from the center of the channel.

In order to avoid gas crossover in the membrane-less electrolyzer

developed here, we make use of the Segré-Silberberg effect on bubbles in the laminar flow regime. A T-junction is used to separate the gas streams at the downstream of a microchannel, after H<sub>2</sub> and O<sub>2</sub> gases are generated at electrodes placed in close proximity to the side walls. A schematic representation of the device is shown in Fig. 2, with pictures of the fabricated device in the inset. In order to ensure a small ohmic potential drop, the inter-electrode distance in the device is kept low, at 105 μm. It is worth noting that this is the only dimension that needs to remain small in order to ensure a laminar flow that provides a steep velocity gradient for the Segré-Silberberg effect to take place. While satisfying this constraint, the electrode dimensions can be freely increased by several orders of magnitudes depending on the available technology, device design and desired application. This dimensionality constraint is equivalent to that in current state of the art electrolyzers which require a very thin MEA to provide low ionic resistivity between the oxygen and hydrogen evolving catalysts, while still allowing a large electrode area in the plane normal to the ion migration pathway. It must be noted that although this study found practical to use a microfluidic platform to explore the potential of the Segré-Silberberg effect on high-performing electrochemical water splitting devices, the principle proposed here can be scaled to devices where large-area

parallel plate electrodes are implemented in order to reach high operating currents, as illustrated in Fig. 1. In this configuration,

the large-area side walls of narrow channels can be coated with appropriate catalysts to achieve higher throughput.

5

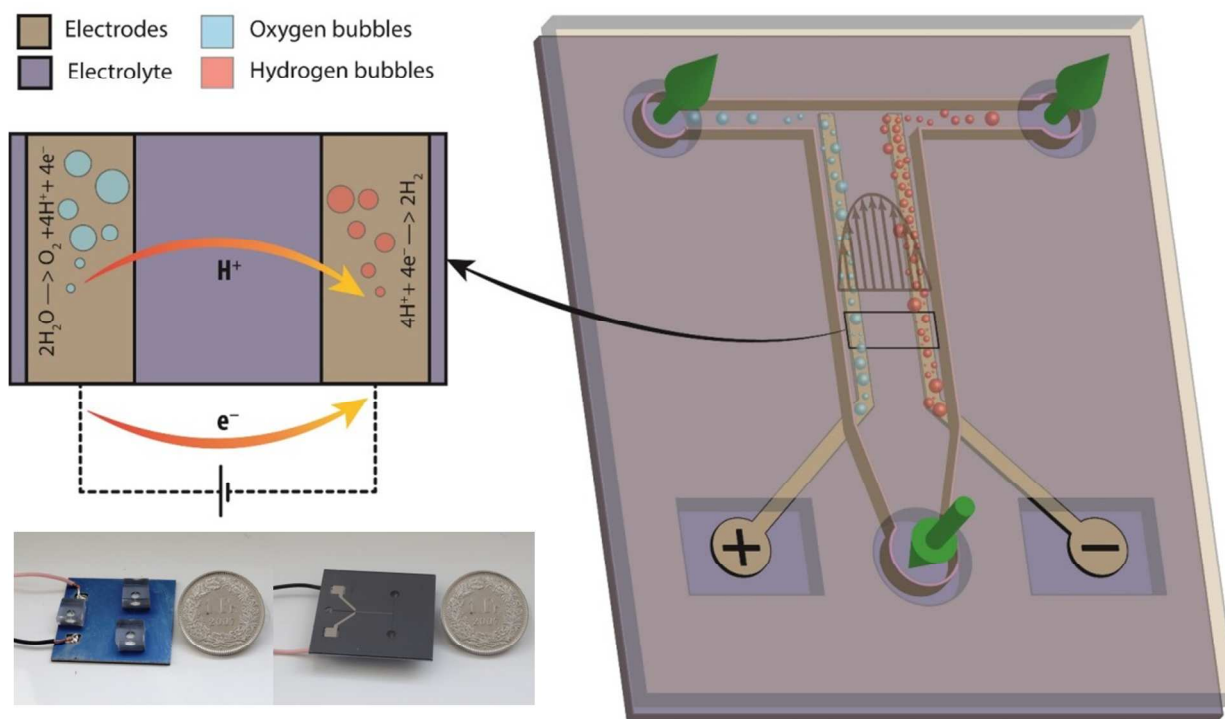


**Fig. 2** Schematic of the proof-of-concept electrolyzer design: hydrogen gas evolves at the cathode (negative electrode) and oxygen gas at the anode (positive electrode). The two gas streams do not experience any convective mixing because of the lift forces that push them towards the neighboring walls. The only mixing mechanism is diffusion of dissolved gases which is minimal at high flow rates. The inset corresponds to photographs of the fabricated device. Fluidic ports and electrical connections can be seen in the left, the electrodes and the T-junction in the right.

10

## Results and discussions

The separation mechanism described above can be visually assessed by tracking the bubbles behavior inside the device. Snapshots of the T-junction are presented in Fig. 3 for devices operating at different flow rates. As the flow rate increases, the size of the bubbles becomes smaller due to the larger drag force at the liquid-gas interface, while the increased inertial lift force keeps the oxygen and hydrogen bubble streams apart. These flow rate effects also fundamentally change the product mixing

mechanism in the device. At low flow rates, convective mixing of bubbles migrating towards the center of the channel dominate the product crossover, while for high flow rates the diffusion of dissolved gases across the electrodes become dominant. This illustrates the important role of inertial lift force in the separation of the two gas streams at high velocities, as observed in the movies S1, S2, and S3 presented in the supplementary information.

20

25

Cite this: DOI: 10.1039/c0xx00000x

www.rsc.org/xxxxxx

ARTICLE TYPE

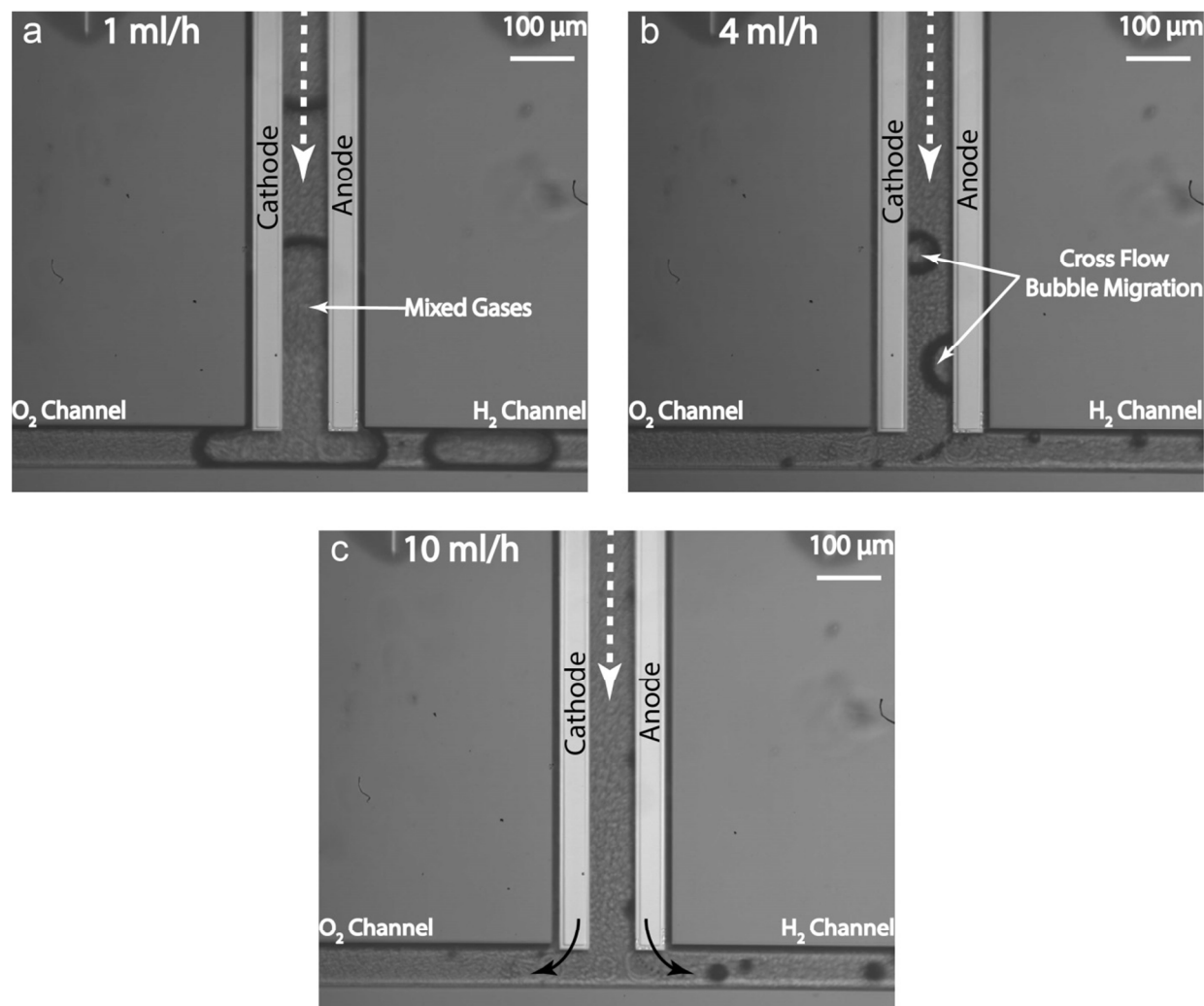


**Fig. 3** Images of the T-junction while the device is working at 143 mA/cm<sup>2</sup> and different flow rates. The two parallel bands are the cathode and the anode, each lying next to a side wall. a: At flow rates of 1 ml/h, the fluidic drag force is so small that the bubbles from the two electrodes grow, coalesce and move out of the device through the two outlets in a mixed form. b: At 4 ml/h, the size of the bubbles is reduced and some of them do not coalesce, although the flow speed is not enough for inertial migration to happen and keep the streams separated. c: At 10 ml/h, gas bubbles are not present in the center of the main channel and each gas stream flows into dedicated outlets. The inertial lift force is sufficient in this case to keep the bubbles close to the side walls.

The membrane-less device demonstrated here shows stable operation at high current densities over the broad range of pH reported in Table S1. The electrochemical performance, as investigated by the device current-voltage characteristics, shows over 300 mA/cm<sup>2</sup> current density with an operating cell voltage of 2.6 V and 14 ml/h flow rate of 1 M sulfuric acid over platinum electrodes. This value can be further improved by integration of a better oxygen evolving catalyst such as iridium oxide and also nanostructuring of the flat electrodes. As presented in Fig. 4a, the effect of the flow rate on the current density is minimal in the range between 8 to 14 ml/h, since the fluidic drag force is high

enough to detach bubbles while they are small, therefore, minimizing the mass transport limitations due to bubbles attached to the electrodes' surface. Additionally, the electrolyzer's behavior in basic and neutral pH electrolytes are shown in Fig. 4b for a flow rate of 12 ml/h. Operating under non-acidic electrolytes is attractive because it opens the possibility to incorporate earth abundant catalysts. To this end, the performance of an electrolyzer with Nickel-Iron (81% Ni, 19% Fe) catalysts was also investigated and reported in Fig. 4b. Furthermore, the device works stably over the course of hours with different electrolytes and catalysts, as shown in Fig. 4c and Fig. S5. This

stable performance is even observed in a Phosphate buffer with pH of 6.6 after an initial equilibrium period of less than few minutes when ionic gradients at the surface of electrodes are expected to be formed. Lastly, it can be inferred from Fig. 4d that the losses in the system are mostly due to reaction kinetics, since ohmic losses stay well below 140 mV, with less than 22 mV arising from solution's ionic resistance at current densities up to

304 mA/cm<sup>2</sup>. It is worth noting that the conductivity of 1 M sulfuric acid is 0.4 S/cm<sup>46</sup> at 25 °C, whereas this parameter for Nafion measured in 1 M sulfuric acid at 25 °C is reported to fall in the range between 0.08 to 0.16 S/cm<sup>47</sup>. This difference shows that the membrane-less device would outperform in efficiency a Nafion-based analogue while still suppressing the gas crossover.

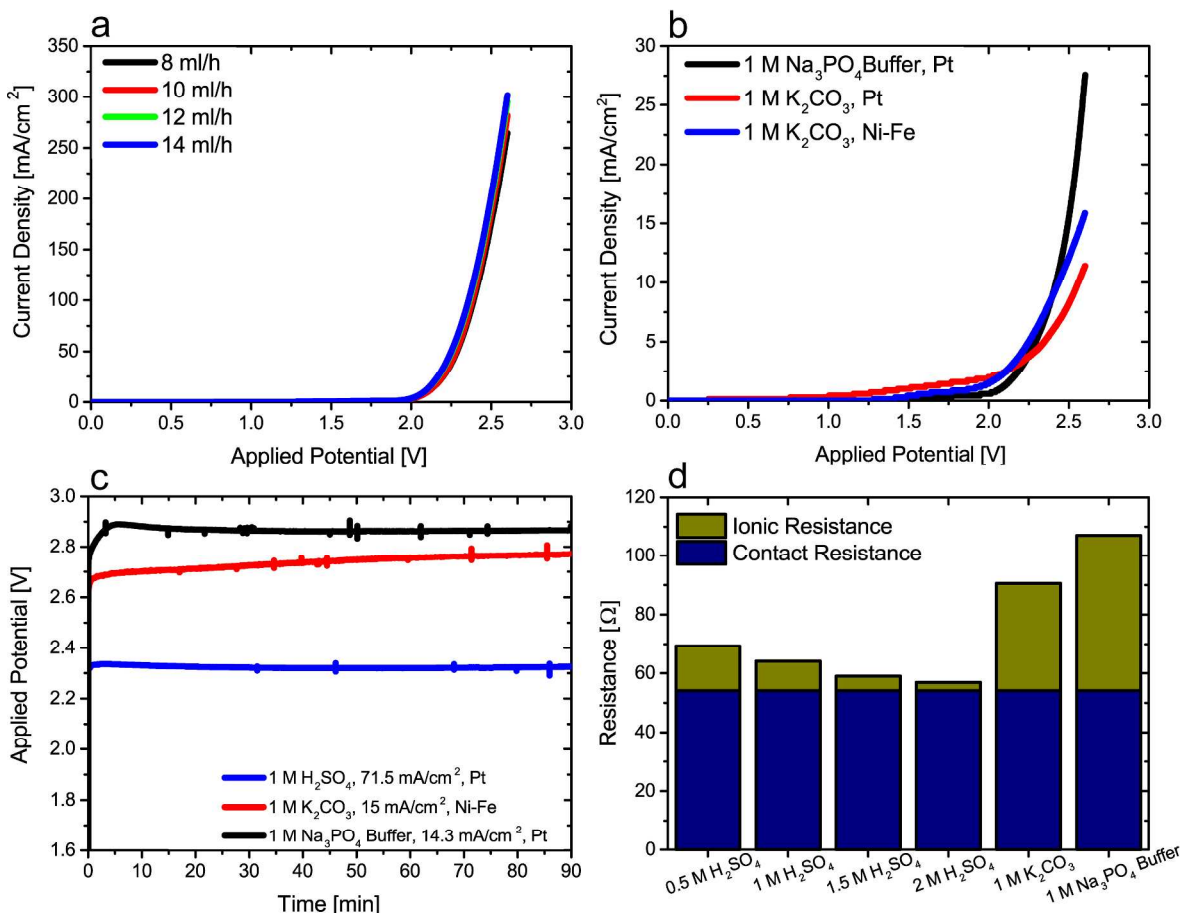


**Fig. 4** Electrochemical characterization of the microdevice. a: Current density as a function of operational voltage for 1 M sulfuric acid at different flow rates. b: J-V characteristics in 1 M Phosphate buffer and Potassium Carbonate with two different catalysts. The current density is smaller than that for acid electrolytes as platinum operates at higher efficiencies at low pH. Also, the results reveal that Ni-Fe outperforms Pt at high pH values. c: The cell voltage remains constant for more than 1.5 hours of operation in 1 M sulfuric acid, Phosphate buffer, and Potassium Carbonate for both Pt and Ni-Fe as catalyst. d: Ohmic resistance for different electrolytes obtained from impedance spectroscopy. Calculations show that the ohmic resistance in the device is mostly due to contact resistance (supplementary information).

The biggest challenge with a membrane-less design is to avoid product mixing which lowers device's efficiency, product's purity and results into a potentially unsafe operation<sup>48</sup>. Fig. 5a shows gas crossover measurements after running the device at 71.5 mA/cm<sup>2</sup> with 1 M sulfuric acid for 90 minutes. The green line shows the maximum allowable crossover to produce non-flammable gas streams, and at flow rates above 12 ml/h the cross contamination is well below this 4% cross contamination threshold. Additionally, volumetric measurements indicate collection efficiencies of up to 91% of H<sub>2</sub> and 93% of O<sub>2</sub> at the outlets of the device. The high collection efficiencies demonstrate minimal losses of the gases due to dissolution in the electrolyte and imperfections in the collection ports. This also indicates that if the electrolyte were to be recycled, the faradaic efficiency would only drop a few percentage points as a consequence of the

recombination of the dissolved gases at the electrodes. At 12 ml/h and 71.5 mA/cm<sup>2</sup>, the ratio between convective flow of H<sub>2</sub> along the channel to its diffusive flow across the channel, predicted by the Peclet number, is higher than  $4.7 \times 10^3$ . In addition, the ratio between the H<sub>2</sub> generation rate and the diffusive flow across the channel is  $1.3 \times 10^8$ . These values show that the H<sub>2</sub> diffusion rate across the electrodes is negligible compared to generation and convective transport rate, indicating that the device is functioning in an appropriate set of operation parameters for purified fuel production, i.e. velocity and current density. The fact that the measured gas crossover is higher than these predicted values suggests that gas mixing in the devices predominantly happens through perturbations that cause convective transport of bubbles across the channel. These perturbations also lead to instabilities in the device electrochemical performance, especially at lower flow

rates as observed in Fig. 5b. When devices operate at low flow rates, bubbles fill the inter-electrode space, increasing the ionic resistance in the device and resulting in fluctuations in the applied potential required to maintain a constant current density. At higher flow rates, the migration of bubbles across the channels is reduced and the ionic resistance between the two electrodes remains constant, resulting in stable operation. It should be noted that requiring high flow rates for gas separation increases the energy required for pumping the fluids. However, the pumping power requirement is estimated to be only 5% of the generated power when the device is operated at 71.5 mA/cm<sup>2</sup> and 12 ml/h (see supplementary information for detailed calculations). These low levels of pumping power can be further reduced by optimizing the channel dimensions in the device.

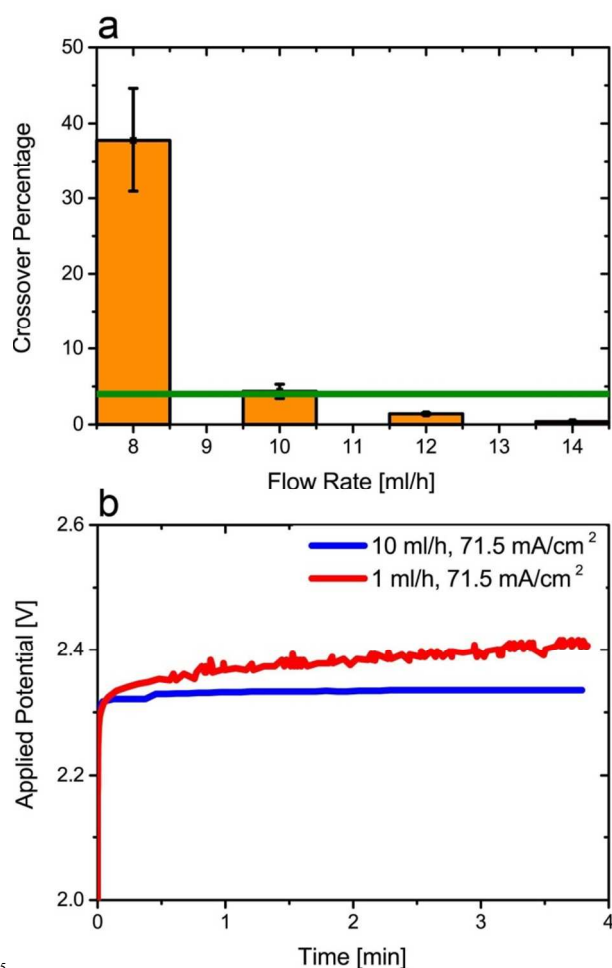


**Fig. 5** a: Gas crossover as a function of flow rate at 71.5 mA/cm<sup>2</sup>. As the flow rate increases the mixing mechanism changes from convection of bubbles to diffusion of dissolved gases. Larger drag force reduces the size of bubbles while the inertial lift force keeps the two bubble streams apart at the same time. b: At low flow rates, the cell voltage fluctuates in order to keep the current density constant. This is due to the changing ionic resistance as the gases displace the electrolyte in the center of the channel.

## Conclusions

The membrane-less electrolyzer demonstrated here has the ability to produce non-flammable hydrogen streams, continuously and stably across the pH scale. Comparing the device ohmic resistance with that for Nafion-based devices, it is clear that this

device has the potential to surpass the performance of similar water splitting apparatus that rely on ion conductive membranes for separation. Although a single electrode pair, such as the one in this proof of concept study, can only produce a limited amount of fuel, scaling it out can be achieved on multi-stack panels for enhanced throughput<sup>49</sup> or the implementation of large area electrodes. As the only dimension to be kept small is the inter-electrode distance, follow up studies are underway to develop high throughput devices where high surface area planar electrodes are used as the side walls of narrow electrolyte channels. Additionally, it is worth noting that this electrolyzer platform may be used in reverse as a fuel cell with two streams of the electrolyte, each saturated with H<sub>2</sub> or O<sub>2</sub>, allowing for the production of electricity<sup>50</sup>. The design simplicity of this membrane-less electrolyzer can facilitate mass production, especially by employing high resolution 3D printers or injection moulding techniques.

## Acknowledgements

The authors acknowledge financial support from grant no. 20NA21-145936 of Nano-Tera Initiative for Solar Hydrogen Integrated Nano Electrolyzer (SHINE) project. They also appreciate the generosity of Professor Haussener's group in EPFL, for facilitating the measurements in the Laboratory of Renewable Energy Science and Engineering. S.M.H.H. would like to thank Jae-Woo Choi, Mikaël Dumortier, Grégoire Laporte, Nicolino Stasio, Ioannis Papadopoulos, Mojtaba Taghipoor, Antonio Delfino, and Sophia Haussener for advice and fruitful discussions.

## Notes and references

- <sup>a</sup> Optics Laboratory, School of Engineering, Swiss Federal Institute of Technology Lausanne (EPFL), CH-1015, Lausanne, Switzerland. E-mail: demetri.psaltis@epfl.ch; Fax: +41 21 6936930; Tel: +41 21 6937795
- <sup>†</sup> Electronic Supplementary Information (ESI) available: [details of any supplementary information available should be included here]. See DOI: 10.1039/b000000x/
- R. M. Navarro, M. A. Pena and J. L. G. Fierro, *Chem Rev*, 2007, **107**, 3952-3991.
  - M. K. Debe, *Nature*, 2012, **486**, 43-51.
  - K. E. Ayers, E. B. Anderson, C. Capuano, B. Carter, L. Dalton, G. Hanlon, J. Manco and M. Niedzwiecki, *ECS Transactions*, 2010, **33**, 3-15.
  - S. Holdcroft, *Chemistry of Materials*, 2013.
  - C. C. L. McCrory, S. Jung, J. C. Peters and T. F. Jaramillo, *Journal of the American Chemical Society*, 2013, **135**, 16977-16987.
  - D. G. Nocera, *Accounts of Chemical Research*, 2012, **45**, 767-776.
  - T. A. Faunce, W. Lubitz, A. W. Rutherford, D. MacFarlane, G. F. Moore, P. Yang, D. G. Nocera, T. A. Moore, D. H. Gregory, S. Fukuzumi, K. B. Yoon, F. A. Armstrong, M. R. Wasielewski and S. Styring, *Energy & Environmental Science*, 2013, **6**, 695-698.
  - N. S. Lewis and D. G. Nocera, *Proceedings of the National Academy of Sciences*, 2006, **103**, 15729-15735.
  - M. G. Walter, E. L. Warren, J. R. McKone, S. W. Boettcher, Q. Mi, E. A. Santori and N. S. Lewis, *Chemical reviews*, 2010, **110**, 6446-6473.
  - S. Y. Reece, J. A. Hamel, K. Sung, T. D. Jarvi, A. J. Esswein, J. J. H. Pijpers and D. G. Nocera, *Science*, 2011, **334**, 645-648.
  - P. W. Du and R. Eisenberg, *Energ Environ Sci*, 2012, **5**, 6012-6021.
  - Q. S. Yin, J. M. Tan, C. Besson, Y. V. Geletii, D. G. Musaev, A. E. Kuznetsov, Z. Luo, K. I. Hardcastle and C. L. Hill, *Science*, 2010, **328**, 342-345.

13. C. R. Cox, J. Z. Lee, D. G. Nocera and T. Buonassisi, *Proceedings of the National Academy of Sciences*, 2014, **111**, 14057-14061.
14. J. Luo, J.-H. Im, M. T. Mayer, M. Schreier, M. K. Nazeeruddin, N.-G. Park, S. D. Tilley, H. J. Fan and M. Grätzel, *Science*, 2014, **345**, 1593-1596.
15. G. Sudre, S. Inceoglu, P. Cotanda and N. P. Balsara, *Macromolecules*, 2013.
16. P. Cotanda, G. Sudre, M. A. Modestino, X. C. Chen and N. P. Balsara, *Macromolecules*, 2014.
17. G. Merle, M. Wessling and K. Nijmeijer, *Journal of Membrane Science*, 2011, **377**, 1-35.
18. G. Couture, A. Alaaeddine, F. Boschet and B. Ameduri, *Progress in Polymer Science*, 2011, **36**, 1521-1557.
19. C. Jangu and T. E. Long, *Polymer*, 2014, **55**, 3298-3304.
20. K. J. T. Noonan, K. M. Hugar, H. A. Kostalik, E. B. Lobkovsky, H. D. Abruña and G. W. Coates, *Journal of the American Chemical Society*, 2012, **134**, 18161-18164.
21. Y. Ye, K. K. Stokes, F. L. Beyer and Y. A. Elabd, *Journal of Membrane Science*, 2013, **443**, 93-99.
22. E. A. Hernandez-Pagan, N. M. Vargas-Barbosa, T. Wang, Y. Zhao, E. S. Smotkin and T. E. Mallouk, *Energy & Environmental Science*, 2012, **5**, 7582-7589.
23. J. Jin, K. Walczak, M. R. Singh, C. Karp, N. S. Lewis and C. Xiang, *Energ Environ Sci*, 2014, **7**, 3371-3380.
24. M. A. Modestino, K. A. Walczak, A. Berger, C. M. Evans, S. Haussener, C. Koval, J. S. Newman, J. W. Ager and R. A. Segalman, *Energy & Environmental Science*, 2014, **7**, 297-301.
25. J. Newman, *Journal of the Electrochemical Society*, 2013, **160**, F309-F311.
26. R. Ferrigno, A. D. Stroock, T. D. Clark, M. Mayer and G. M. Whitesides, *J Am Chem Soc*, 2002, **124**, 12930-12931.
27. E. R. Choban, L. J. Markoski, A. Wieckowski and P. J. A. Kenis, *J Power Sources*, 2004, **128**, 54-60.
28. R. S. Jayashree, L. Gancs, E. R. Choban, A. Primak, D. Natarajan, L. J. Markoski and P. J. A. Kenis, *J Am Chem Soc*, 2005, **127**, 16758-16759.
29. F. R. Brushett, W. P. Zhou, R. S. Jayashree and P. J. A. Kenis, *J Electrochem Soc*, 2009, **156**, B565-B571.
30. N. Da Mota, D. A. Finkelstein, J. D. Kirtland, C. A. Rodriguez, A. D. Stroock and H. D. Abruña, *J Am Chem Soc*, 2012, **134**, 6076-6079.
31. E. Kjeang, R. Michel, D. A. Harrington, N. Djilali and D. Sinton, *J Am Chem Soc*, 2008, **130**, 4000-4006.
32. E. Kjeang, B. T. Proctor, A. G. Brolo, D. A. Harrington, N. Djilali and D. Sinton, *Electrochim Acta*, 2007, **52**, 4942-4946.
33. J. L. Cohen, D. A. Westly, A. Pechenik and H. D. Abruña, *J Power Sources*, 2005, **139**, 96-105.
34. W. A. Braff, M. Z. Bazant and C. R. Buie, *Nat Commun*, 2013, **4**.
35. Y. Yang, J. Loomis, H. Ghasemi, S. W. Lee, Y. J. Wang, Y. Cui and G. Chen, *Nano Letters*, 2014.
36. G. Segre and A. Silberberg, *J Fluid Mech*, 1962, **14**, 115-135.
37. G. Segre and A. Silberberg, *J Fluid Mech*, 1962, **14**, 136-157.
38. J. A. Schonberg and E. J. Hinch, *J Fluid Mech*, 1989, **203**, 517-524.
39. J. B. McLaughlin, *J Fluid Mech*, 1991, **224**, 261-274.
40. J. B. McLaughlin, *J Fluid Mech*, 1993, **246**, 249-265.
41. G. Segre and A. Silberberg, *Nature*, 1961, **189**, 209-&.
42. A. A. S. Bhagat, S. S. Kuntaegowdanahalli and I. Papautsky, *Phys Fluids*, 2008, **20**.
43. D. Di Carlo, *Lab Chip*, 2009, **9**, 3038-3046.
44. S. S. Kuntaegowdanahalli, A. A. S. Bhagat, G. Kumar and I. Papautsky, *Lab Chip*, 2009, **9**, 2973-2980.
45. H. Amini, W. Lee and D. Di Carlo, *Lab Chip*, 2014, **14**, 2739-2761.
46. H. E. Darling, *Journal of Chemical & Engineering Data*, 1964, **9**, 421-426.
47. S. Slade, S. A. Campbell, T. R. Ralph and F. C. Walsh, *J Electrochem Soc*, 2002, **149**, A1556-A1564.
48. A. Berger, R. A. Segalman and J. Newman, *Energ Environ Sci*, 2014, **7**, 1468-1476.
49. K. S. Elvira, X. C. I. Solvas, R. C. R. Wootton and A. J. deMello, *Nat Chem*, 2013, **5**, 905-915.
50. J. L. Cohen, D. J. Volpe, D. A. Westly, A. Pechenik and H. D. Abruña, *Langmuir*, 2005, **21**, 3544-3550.

### Broader Context

Ion conductive membranes are considered as an essential component in water electrolyzers. Since its introduction in 1960s, Nafion<sup>®</sup> has become the benchmark proton conducting membrane in both industrial and academic settings. Despite its high price, limited life time and limitation to strongly acidic pHs, researchers have adopted this material mainly due to its superior stability and ion conductivity. Membrane-less electrolysis schemes can address these challenges and lead to even more efficient devices thanks to the higher conductivity of liquid electrolytes. This study demonstrates for the first time a membrane-less device which can operate robustly and continuously with various catalysts and electrolytes across the pH scale, while at the same time generating Hydrogen gas streams whose Oxygen content is well below the safety limit.